On the Implementation of Fuzzy VMC for an Under Actuated System

SABRI BICAKCI [ID], (Member, IEEE)

Mechatronics Engineering Department, Balıkesir University, 10145 Balıkesir, Turkey

e-mail: sbicakci@balikesir.edu.tr

ABSTRACT Most of control strategies are based on complex mathematical equations and the success of them is directly related to the precise acquisition of the mathematical model of the system. Virtual Model Control (VMC) allows the system to be mechanically controlled like a puppet with intuitive approaches instead of complex mathematical equations. In this paper, a novel implementation of fuzzy VMC on inverted pendulum, which is an under actuated mechanism, is presented. The cart of the inverted pendulum is controlled by manipulating the vertical equilibrium point of the pendulum with two cascaded VMCs. A Takagi-Sugeno fuzzy parameter tuner is designed to improve the VMC performance. An LQR controller is also designed to compare the performances of the controllers. The complete control system is implemented on FPGA based embedded platform in real time. The simulation and experimental results indicated that the proposed VMC successfully controls the inverted pendulum. In addition, the VMC with fuzzy parameter tuner has lower rise time, settling time, IAE and ITAE when compared to the LQR which is widely used controller in the literature.

INDEX TERMS Fuzzy logic, inverted pendulum, parameter tuner, virtual model control.

I. INTRODUCTION

Inverted pendulum mechanism is mostly used as a benchmark system for control algorithms because of its nonlinear and under actuated nature. Wide variety of control techniques have been used to control this mechanism such as PID (Proportional, Integral and Derivative) [1]–[3], [44], [46], LQR (Linear Quadratic Regulator) [4], [5], Sliding Mode Control [6]–[11], Backstepping Control [12], [13], [45], Grey Prediction Control [14], Energy Based Control [15], [16], FLC (Fuzzy Logic Control) [17]–[20], NN (Neural Network) [21] and ANFIS (Adaptive Neuro-Fuzzy Inference System) [22], [23]. Most of these control strategies are based on complex mathematical equations and the success of them is directly proportional to the precise acquisition of the mathematical model of the system [24]. Virtual Model Control (VMC) firstly introduced by Pratt and his colleagues [25] allows the system to be mechanically controlled like a puppet with intuitive approaches instead of complex mathematical equations. To design the VMC, one needs to imagine that how the system can be controlled using mechanical components

such as spring, suspension, mass so on. Thus, it is required to realize the actions of virtual components with real actuator using basic kinematic equations. For instance, if a spring is connected between a base point and a cart, which can be moved on a linear slide with the DC motor actuator, the cart will oscillate around rest position of the spring. In addition, the cart can be held in the resting position without oscillation when a suspension is added to this mechanism. Since the spring and suspension are virtual, proper voltages must be applied to the DC motor to realize the actions of the virtual components. Pioneer studies on the VMC were made in the MIT Leg Laboratory. A simulated hexapod [25] and two different types of bipedal walking robot [26], [27] were controlled using the VMC. An adaptive VMC for a simulated biped robot was also been developed based on the sliding control theory [28]. In the researches by others, applicability of the VMC were investigated over the humanoid robots [29], legged robots [30], [31], quadruped robots [32]–[34], exoskeletons [35], [36] and articulated landing gear [37]. It should be noted that there are no experimental studies on under actuated system control using the VMC.

The parameters of the control system require to be adjusted for the proper implementation of the control strategies.
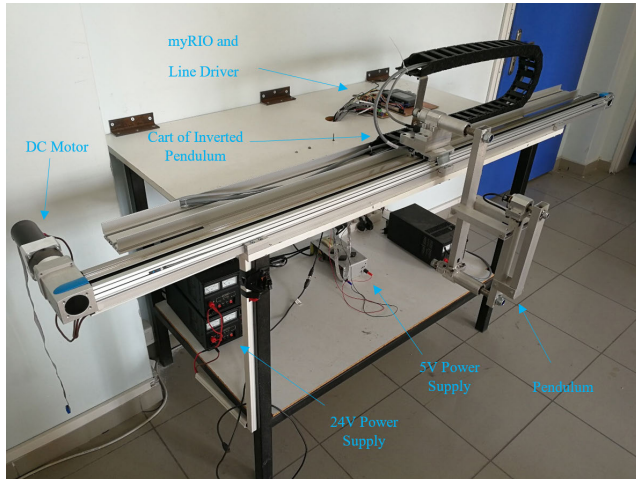
The associate editor coordinating the review of this manuscript and approving it for publication was Min Wang [ID].

FIGURE 1. Inverted pendulum mechanism.

The adjusting VMC parameters is much practical than those of other control techniques and can be done experimentally, since the changes in the parameters of the virtual mechanical components effect the system as if the components are physically on the system. Thus, the control performance can be improved changing the control parameters depending on the dynamics of system [38]. This also allows the controller to adapt to system uncertainties. The dynamical control parameter tuning studies are focused on fuzzy [24], [38], [39] and neuro-fuzzy [22], [40], [41] methods because of their nonlinear and dynamic capabilities.

In this paper, an inverted pendulum is controlled using the VMC technique and the control parameters are adjusted adaptively using fuzzy logic. An LQR controller is also designed for the inverted pendulum and the results of the controllers are comparatively evaluated. In the second section of the paper, the designed and manufactured inverted pendulum system is introduced particularly. In the following sections, the control system design and fuzzy parameter tuning system are described respectively. Finally, experimental results are evaluated and conclusion of the study are presented.

II. THE EXPERIMENTAL SETUP AND THE MATHEMATICAL MODEL

The designed and manufactured inverted pendulum mechanism used as an experimental setup, which consists of a cart on a linear slide and a pendulum attached to the cart, is shown in Fig. 1. The mechanism has three rotational and one linear axes. Two rotational axes are fixed mechanically since this study aims to stabilize only one rotational axis.

Festo EGC-TB-KF series linear slide with 1800 mm stroke is used as the linear axis. The cart on the slide is actuated along the axis using a Maxon RE50 200 Watt, 24V DC motor with gearbox via toothed belt and pulley mechanism. The cart position and the pendulum angle are measured respectively using linear incremental encoder with 0.025 mm resolution and rotary incremental encoder with 3.142e-4 radians (0.018 degrees) resolution.
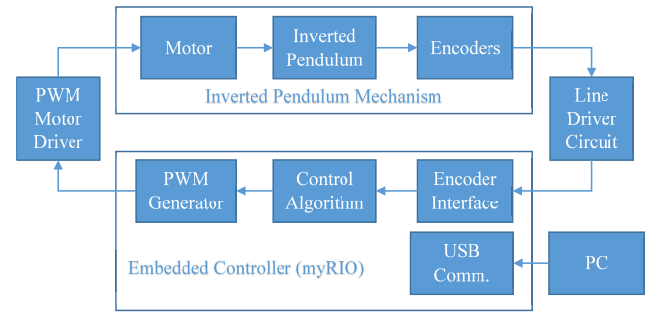

FIGURE 2. Complete experimental system schematic.

Schematic of the complete experimental system is shown in Fig. 2. The myRIO platform [43], which has ARM Cortex A9 processor and Xilinx Zynq 7 Series FPGA, is used as an embedded controller. The encoder signals are fed to encoder interface module of the myRIO platform via line driver circuit for measuring positions of the cart and the pendulum. The objective of the controller is to control the position of the cart with desired reference position signal while balancing the pendulum in the upright equilibrium point. The reference position signals are generated programmatically in the embedded controller. The control signals acquired from the control algorithm are transformed to the PWM signals by PWM generator and applied to the motor via Pololu 24v23 CS PWM motor driver (24V, 500W). The myRIO embedded platform is programmed using Labview graphical programming software. The PC is only used for changing the control parameters, monitoring and logging the system parameters in real time.

The mathematical model of the inverted pendulum mechanism required for the simulations, which is derived using free body diagram, is given in Eq. (1) and Eq. (2),

$$(m \cdot l^2 + I) \cdot \ddot{\theta} = m \cdot g \cdot l \cdot \sin\theta + \ddot{x} \cdot m \cdot l \cdot \cos\theta - F_{fp} \cdot \dot{\theta} \tag{1}$$

$$(M + m) \cdot \ddot{x} = F_{motor} + \ddot{\theta} \cdot m \cdot l \cdot \cos\theta - m \cdot l$$
$$\cdot \dot{\theta}^2 \cdot \sin\theta - F_{fc} \cdot \dot{x} \tag{2}$$

where m is the mass of the pendulum, M is the mass of the cart, θ is the rotation angle of the pendulum, x is the position of the cart, l is the length of the centre of the gravity of the pendulum, I is the moment of the inertia of the pendulum, g is the gravitational acceleration, F_{fp} is the viscous friction constant of the pendulum, F_{fc} is the viscous friction constant of the cart and F_{motor} is the force applied to the cart by the DC motor and can be calculated by means of the Eq. (3).

$$F_{motor} = A \cdot V - B \cdot \dot{x} - C \cdot \ddot{x} \tag{3}$$

where A, B and C coefficients are given by Eq. (4).

$$A = \frac{N \cdot \eta \cdot K_t}{R_a \cdot r}; \quad B = \frac{N^2 \cdot \eta \cdot K_t \cdot K_b}{R_a \cdot r^2}; \quad C = \frac{N^2 \cdot \eta \cdot J_m}{r^2} \tag{4}$$

TABLE 1. The Pendulum parameters.

Symbol	Quantity	Value
m	the pendulum mass	2.09838 kg
l	the length of the gravity centre	0.25535 m
I	the moment of the inertia	0.05052 kg.m^2
g	the gravitational acceleration	9.81 m/s^2
M	the cart mass	1.70411 kg
r	the radius of the pulley	0.012415 m
N	the gear ratio	8
η	the efficiency of the DC motor	0.90
K_t	the torque constant	0.0385 N.m/A
K_b	the back electromotive force constant	0.0385 V.s/rad
R_a	the armature resistant of the motor	0.103 ohm
J_m	the moment of inertia of the motor	6.03e-5 kg.m^2
F_{fp}	the viscous friction constant of the pendulum	0
F_{fc}	the viscous friction constant of the cart	72.49 N.s/m

In Eq. (4), r is the radius of the pulley that is mounted on the shaft of the motor, N is the gear ratio, η is the efficiency of the DC motor, K_t the torque constant, K_b is the back electromotive force constant, R_a is the armature resistant of the motor, J_m is the moment of inertia of the motor, x is the position of the cart and V is the voltage applied to the DC motor. The motor parameters (K_t, K_b, R_a and J_m) are provided from the motor catalogue [42]. The parameter values of the mechanical system are given in Table 1.

If state variables of the system are selected as;

$$X = [x_1\, x_2\, x_3\, x_4]^t = \left[x\, \theta\, \dot{x}\, \dot{\theta}\right]^t \tag{5}$$

the nonlinear state equations of the system easily derived from Eq. (1) - (3) can be written as;

$$\begin{bmatrix} \dot{x}_1 \\ \dot{x}_2 \\ \dot{x}_3 \\ \dot{x}_4 \end{bmatrix} = \begin{bmatrix} x_3 \\ x_4 \\ f_1(x) + g_1(x) \cdot V \\ f_2(x) + g_2(x) \cdot V \end{bmatrix} \tag{6}$$

where $f_1(x)$, $g_1(x)$, $f_2(x)$ and $g_2(x)$ are derived by

$$f_1(x) = \frac{m^2 \cdot l^2 \cdot g \cdot \cos x_2 \cdot \sin x_2}{(M+m+C) \cdot (m \cdot l^2 + I) - (m \cdot l \cdot \cos x_2)^2}$$
$$- \frac{(B+F_{fc}) \cdot (m \cdot l^2 + I)}{(M+m+C) \cdot (m \cdot l^2 + I) - (m \cdot l \cdot \cos x_2)^2} \cdot x_3$$
$$- \frac{m \cdot l \cdot \cos x_2 \cdot F_{fp}}{(M+m+C) \cdot (m \cdot l^2 + I) - (m \cdot l \cdot \cos x_2)^2} \cdot x_4$$
$$- \frac{(m \cdot l \cdot \sin x_2) \cdot (m \cdot l^2 + I)}{(M+m+C) \cdot (m \cdot l^2 + I) - (m \cdot l \cdot \cos x_2)^2} \cdot x_4^2$$

$$g_1(x) = \frac{A \cdot (m \cdot l^2 + I)}{(M+m+C) \cdot (m \cdot l^2 + I) - (m \cdot l \cdot \cos x_2)^2}$$

$$f_2(x) = \frac{(M+m+C) \cdot m \cdot g \cdot l \cdot \sin x_2}{(M+m+C) \cdot (m \cdot l^2 + I) - (m \cdot l \cdot \cos x_2)^2}$$
$$- \frac{(B+F_{fc}) \cdot m \cdot l \cdot \cos x_2}{(M+m+C) \cdot (m \cdot l^2 + I) - (m \cdot l \cdot \cos x_2)^2} \cdot x_3$$
$$- \frac{(M+m+C) \cdot F_{fp}}{(M+m+C) \cdot (m \cdot l^2 + I) - (m \cdot l \cdot \cos x_2)^2} \cdot x_4$$
$$- \frac{m^2 \cdot l^2 \cdot \cos x_2 \cdot \sin x_2}{(M+m+C) \cdot (m \cdot l^2 + I) - (m \cdot l \cdot \cos x_2)^2} \cdot x_4^2$$

$$g_2(x) = \frac{A \cdot m \cdot l \cdot \cos x_2}{(M+m+C) \cdot (m \cdot l^2 + I) - (m \cdot l \cdot \cos x_2)^2} \tag{7}$$

The system can be linearized near $x_2 = 0$ and the state equations can be written as;

$$\begin{bmatrix} \dot{x}_1 \\ \dot{x}_2 \\ \dot{x}_3 \\ \dot{x}_4 \end{bmatrix} = \begin{bmatrix} 0 & 0 & 1 & 0 \\ 0 & 0 & 0 & 1 \\ 0 & a_{32} & a_{33} & a_{34} \\ 0 & a_{42} & a_{43} & a_{44} \end{bmatrix} \begin{bmatrix} x_1 \\ x_2 \\ x_3 \\ x_4 \end{bmatrix} + \begin{bmatrix} 0 \\ 0 \\ b_1 \\ b_2 \end{bmatrix} \cdot V$$

$$a_{32} = \frac{m^2 \cdot l^2 \cdot g}{(M+m+C) \cdot (m \cdot l^2 + I) - (m \cdot l)^2};$$

$$a_{33} = -\frac{(B+F_{fc}) \cdot (m \cdot l^2 + I)}{(M+m+C) \cdot (m \cdot l^2 + I) - (m \cdot l)^2};$$

$$a_{34} = -\frac{m \cdot l \cdot F_{fp}}{(M+m+C) \cdot (m \cdot l^2 + I) - (m \cdot l)^2};$$

$$a_{42} = \frac{(M+m+C) \cdot m \cdot g \cdot l}{(M+m+C) \cdot (m \cdot l^2 + I) - (m \cdot l)^2};$$

$$a_{43} = -\frac{(B+F_{fc}) \cdot m \cdot l}{(M+m+C) \cdot (m \cdot l^2 + I) - (m \cdot l)^2};$$

$$a_{44} = -\frac{(M+m+C) \cdot F_{fp}}{(M+m+C) \cdot (m \cdot l^2 + I) - (m \cdot l)^2};$$

$$b_1 = \frac{A \cdot (m \cdot l^2 + I)}{(M+m+C) \cdot (m \cdot l^2 + I) - (m \cdot l)^2};$$

$$b_2 = \frac{A \cdot m \cdot l}{(M+m+C) \cdot (m \cdot l^2 + I) - (m \cdot l)^2} \tag{8}$$

By substituting numerical values of the parameters given in Table 1 to Eq. (8), the state space equations of the complete mechanical system are found as in Eq.(9).

$$\begin{bmatrix} \dot{x}_1 \\ \dot{x}_2 \\ \dot{x}_3 \\ \dot{x}_4 \end{bmatrix} = \begin{bmatrix} 0 & 0 & 1 & 0 \\ 0 & 0 & 0 & 1 \\ 0 & 0.6061 & -219.7351 & 0 \\ 0 & 29.7913 & -628.4698 & 0 \end{bmatrix}$$
$$\times \begin{bmatrix} x_1 \\ x_2 \\ x_3 \\ x_4 \end{bmatrix} + \begin{bmatrix} 0 \\ 0 \\ 8.7394 \\ 24.9957 \end{bmatrix} \cdot V \tag{9}$$

III. VIRTUAL MODEL CONTROLLER

The VMC design consists of three main steps. The first step is to imagine and attach virtual components to the system, which is aimed to be controlled. The second step is to obtain the virtual forces and torques that must occur in the joints. The last step is deriving the real actuator equations to realize the virtual forces and torques [25], [26].
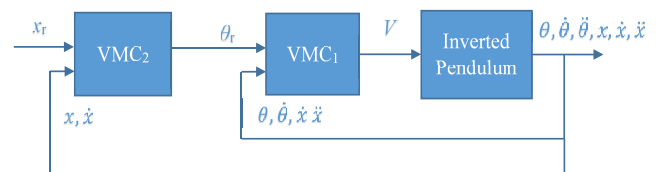

FIGURE 3. Block diagram of the designed virtual model controller.

Two level cascaded VMC shown in Fig. 3 is designed to control the inverted pendulum.
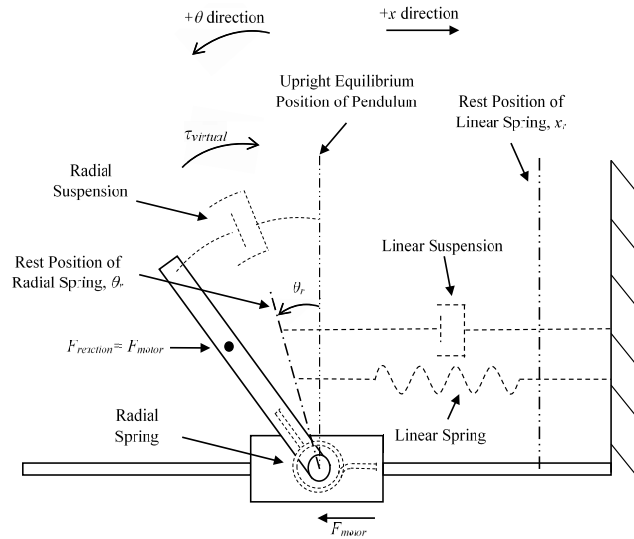
FIGURE 4. Virtual components attached to the inverted pendulum.

The VMC$_1$ is designed to stabilize the pendulum around the upright equilibrium position and the VMC$_2$ is employed to control the position of the cart. Fig. 4 shows the illustration of where the imagined virtual components of the VMC$_1$ and VMC$_2$ are attached on the inverted pendulum. The VMC$_1$ consists of a virtual radial spring and suspension pair, which is connected between the pendulum and the cart. When the rest position of the virtual radial spring (θ_r) is set to zero radians (the upright equilibrium point), the spring generates virtual torque to hold the pendulum at that position. And virtual radial suspension generates virtual torque to damp the oscillations around the rest position of the spring. If angle of the pendulum shifts from the vertical equilibrium to any direction, the virtual torque of the spring forms in the opposed direction of the shift.

These virtual torques can only be realized by reaction force ($F_{reaction}$) on the pendulum caused by the movement of the cart. The $F_{reaction}$ is equal to the force generated by the DC motor (F_{motor}) but is in the opposite direction of the movement. So to create the total virtual torque ($\tau_{virtual}$) generated by the virtual radial spring and suspension pair expressed in Eq. (10), the cart must be moved in the opposite direction.

$$\tau_{virtual} = K_r \cdot (\theta_r - \theta) - B_r \cdot \dot{\theta} \qquad (10)$$

where K_r is the constant of the radial spring, B_r is the damping coefficient of the radial suspension, θ_r is the rest position of the radial spring, and θ is the angle of the pendulum. The voltage, which should be applied to the DC motor in order to form the total virtual torque, can be obtained from Eq. (14).

$$\tau_{reaction} = F_{motor} \cdot l \cdot \cos \theta \qquad (11)$$

$$\tau_{reaction} = \tau_{virtual} \qquad (12)$$

$$F_{motor} = \frac{\tau_{virtual}}{l \cdot \cos \theta} = \frac{K_r \cdot (\theta_r - \theta) - B_r \cdot \dot{\theta}}{l \cdot \cos \theta} \qquad (13)$$

$$V = \frac{B}{A} \cdot \dot{x} + \frac{C}{A} \cdot \ddot{x} + \frac{K_r \cdot (\theta_r - \theta) - B_r \cdot \dot{\theta}}{A \cdot l \cdot \cos \theta} \qquad (14)$$

Here $\tau_{reaction}$ is the torque caused by $F_{reaction}$ and l is the length of the centre of mass of the pendulum.

If θ_r is shifted from zero radians to any direction, the VMC$_1$ will continuously move the cart in the corresponding direction to stabilize the pendulum in this position by overcoming the gravity. The position of the cart can be controlled using this effect of the VMC$_1$. Therefore, the VMC$_2$ is designed as a reference generator for the VMC$_1$. A virtual linear spring and suspension pair is connected between the θ_r and the fixed end point of the linear axis to form the VMC$_2$. When the rest position of the linear spring (x_r) is shifted towards the desired cart position as the amount of position error of the cart, a virtual action is generated by the linear spring to cause θ_r to shift in the corresponding direction. The linear suspension also produces the virtual action to damp the oscillations in θ_r. The equation used to calculate θ_r as the output of VMC$_2$ is given in Eq. (15).

$$\theta_r = -K_l \cdot (x_r - x) + B_l \cdot \dot{x} \qquad (15)$$

where K_l is the constant of the linear spring, B_l is the damping coefficient of the linear suspension, x_r is the rest position of the linear spring and x is the position of the cart.

By substituting Eq. (14) and Eq. (15) to Eq. (6), final nonlinear state equations of the system can be written as;

$$\begin{bmatrix} \dot{x}_1 \\ \dot{x}_2 \\ \dot{x}_3 \\ \dot{x}_4 \end{bmatrix} = \begin{bmatrix} x_3 \\ x_4 \\ f_3(x) + g_3(x) \cdot x_r \\ f_4(x) + g_4(x) \cdot x_r \end{bmatrix} \qquad (16)$$

where $f_3(x), g_3(x), f_4(x)$ and $g_4(x)$ are derived by

$$\begin{aligned}
f_3(x) = & \frac{m^2 \cdot l^2 \cdot g \cdot \cos x_2 \cdot \sin x_2}{(M+m) \cdot (m \cdot l^2 + I) - (m \cdot l \cdot \cos x_2)^2} \\
& + \frac{K_r \cdot K_l \cdot (m \cdot l^2 + I)}{l \cdot \cos x_2 \cdot [(M+m) \cdot (m \cdot l^2 + I) - (m \cdot l \cdot \cos x_2)^2]} \cdot x_1 \\
& - \frac{K_r \cdot (m \cdot l^2 + I)}{l \cdot \cos x_2 \cdot [(M+m) \cdot (m \cdot l^2 + I) - (m \cdot l \cdot \cos x_2)^2]} \cdot x_2 \\
& + \frac{(m \cdot l^2 + I) \cdot (K_r \cdot B_l - l \cdot \cos x_2 \cdot F_{fc})}{l \cdot \cos x_2 \cdot [(M+m) \cdot (m \cdot l^2 + I) - (m \cdot l \cdot \cos x_2)^2]} \cdot x_3 \\
& - \frac{B_r \cdot (m \cdot l^2 + I) + m \cdot (l \cdot \cos x_2)^2 \cdot F_{fp}}{l \cdot \cos x_2 \cdot [(M+m) \cdot (m \cdot l^2 + I) - (m \cdot l \cdot \cos x_2)^2]} \cdot x_4 \\
& - \frac{(m \cdot l \cdot \sin x_2) \cdot (m \cdot l^2 + I)}{(M+m) \cdot (m \cdot l^2 + I) - (m \cdot l \cdot \cos x_2)^2} \cdot x_4^2
\end{aligned}$$

$$g_3(x) = -\frac{K_r \cdot K_l \cdot (m \cdot l^2 + I)}{l \cdot \cos x_2 \cdot [(M+m) \cdot (m \cdot l^2 + I) - (m \cdot l \cdot \cos x_2)^2]}$$

$$\begin{aligned}
f_4(x) = & \frac{(M+m) \cdot m \cdot g \cdot l \cdot \sin x_2}{(M+m) \cdot (m \cdot l^2 + I) - (m \cdot l \cdot \cos x_2)^2} \\
& + \frac{K_r \cdot K_l \cdot m}{(M+m) \cdot (m \cdot l^2 + I) - (m \cdot l \cdot \cos x_2)^2} \cdot x_1 \\
& - \frac{K_r \cdot m}{(M+m) \cdot (m \cdot l^2 + I) - (m \cdot l \cdot \cos x_2)^2} \cdot x_2
\end{aligned}$$

FIGURE 5. Block diagram of the FPT.

$$+\frac{m \cdot (K_r \cdot B_l - l \cdot \cos x_2 \cdot F_{fc})}{(M+m) \cdot (m \cdot l^2 + I) - (m \cdot l \cdot \cos x_2)^2} \cdot x_3$$

$$-\frac{m \cdot B_r + (M+m) \cdot F_{fp}}{(M+m) \cdot (m \cdot l^2 + I) - (m \cdot l \cdot \cos x_2)^2} \cdot x_4$$

$$-\frac{m^2 \cdot l^2 \cdot \cos x_2 \cdot \sin x_2}{(M+m) \cdot (m \cdot l^2 + I) - (m \cdot l \cdot \cos x_2)^2} \cdot x_4^2$$

$$g_2(x) = -\frac{K_r \cdot K_l \cdot m}{(M+m) \cdot (m \cdot l^2 + I) - (m \cdot l \cdot \cos x_2)^2} \quad (17)$$

If the Eq. 16 is linearized near $x_2 = 0$, the characteristic equation of the system given in Eq. 18 can be easily obtained by using the numerical values of the parameters given in Table 1.

$$s^4 + (31.9343 - 1.7252 \cdot K_r \cdot B_l + 4.9343 \cdot B_r) \cdot s^3$$
$$+ (4.9343 \cdot K_r - 1.7252 \cdot K_r \cdot K_l - 47.003) \cdot s^2$$
$$+ (48.4058 \cdot K_r \cdot B_l - 896.0063) \cdot s$$
$$+ 48.4058 \cdot K_r \cdot K_l = 0 \quad (18)$$

If Routh-Hurwitz stability analysis is performed, it is clearly seen that all parameters of the controller (K_r, B_r, K_l and B_l) must be selected greater than zero. If K_r and B_r values are selected as 8000 and 1150 respectively (see Table 4), K_l and B_l values must be chosen according to the rules given in Eq. 19 to guaranty the stability of the control system.

$$0.4135 > B_l > 0.0023$$
$$2.8557 > K_l > 0 \quad (19)$$

IV. FUZZY PARAMETER TUNING SYSTEM

Due to the nonlinearity of system, the controller performance can be improved by dynamically changing the control parameters depending upon the dynamics of the system. It also allows the controller to adapt to system uncertainties. The dynamic parameter changes made in the VMC_2 will also affect the VMC_1 since the control system proposed in this study is cascaded. Thus, a Takagi-Sugeno Type Zero [18], [19] fuzzy parameter tuner (FPT) is designed for the VMC_2. The block diagram of the FPT is shown in Fig.5.

The crisp inputs of the FPT are the error of the cart position - e_x and the change in the error - $\dot{e}_x$. The crisp outputs of FPT are the constant of the linear spring, K_l and the damping coefficient of the linear suspension, B_l. The membership functions given in Fig. 6 are used to fuzzify the inputs of FPT.

Five triangular membership functions (Negative Big – NB, Negative Small – NS, Zero – Z, Positive Small – PS, Positive Big – PB), which are selected for e_x. NB – PB, NS – PS and Z membership functions, are the acceleration, the braking and the small error zones for the cart, respectively. In order to determine the direction and the amount of change in the error, three triangular membership functions (Negative – N,
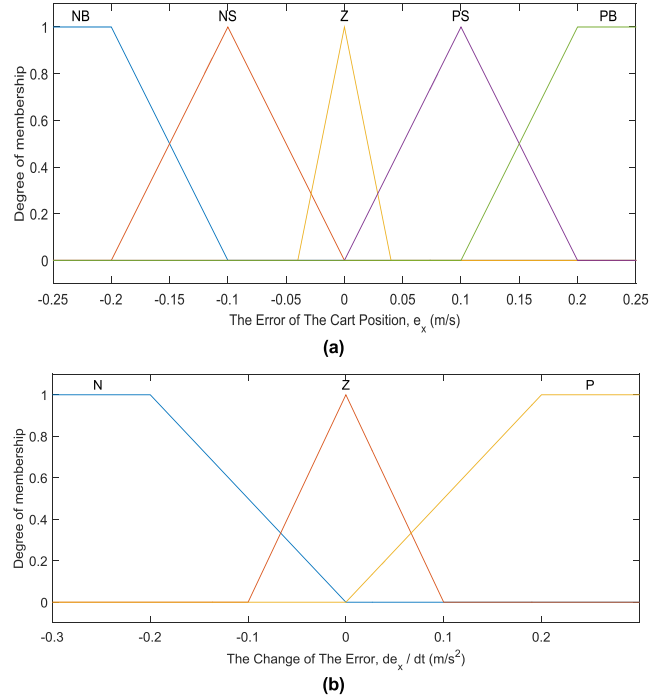

FIGURE 6. The membership functions of the inputs of the FPT. (a) The membership function of e_x. (b) The membership function of $\dot{e}_x$.

TABLE 2. The rule bases of the FPT.

a)

		Membership function of the $\dot{e}_x$		
		N	Z	P
Membership function of the e_x	NB	B	B	B
	NS	M	S	S
	Z	S	S	S
	PS	S	S	M
	PB	B	B	B

b)

		Membership function of the $\dot{e}_x$		
		N	Z	P
Membership function of the e_x	NB	B	M	S
	NS	B	B	B
	Z	M	S	M
	PS	B	B	B
	PB	S	M	B

Zero – Z, Positive – P) are selected for $\dot{e}_x$. The outputs of the FPT are generated based on the fifteen element rule bases given in Table 2 by using three levelled singleton membership functions (Small – S, Medium – M and Big – B).

The crisp outputs of the FPT are calculated by means of the weighted average of all rule outputs method given in Eq. (20) and the selected values of the membership functions of the outputs given in Table 3. The values of the membership functions of Kl and Bl are selected in according to Eq. 19.

$$Output = \frac{\sum\limits_{i=1}^{15} w_i \cdot z_i}{\sum\limits_{i=1}^{15} w_i} \quad (20)$$

where the w_i's are the firing strengths of the rules and z_i's are the values of the membership functions of the outputs.

TABLE 3. The values of the membership functions of the outputs.

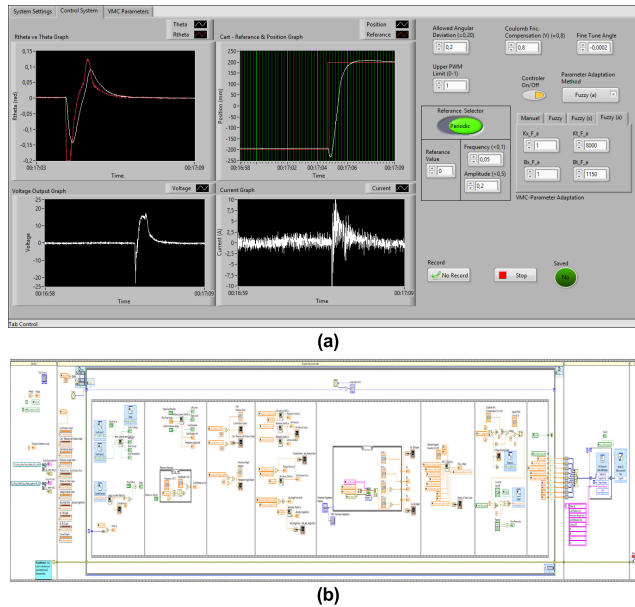| Membership functions	For the K_l output	For the B_l output
S	0.245	0.2369
M	0.2744	0.2575
B	0.392	0.2781

(a)

(b)

FIGURE 7. The front panel and block diagram view of the implementation program in Labview. (a) The front panel of the implementation program. (b) Block diagram of the implementation program.

V. SIMULATED AND EXPERIMENTAL RESULTS

Experimental and simulated tests are conducted to demonstrate the performance of the proposed VMC system and the FPT. The control algorithm is implemented on myRIO embedded platform using Labview software for experimental tests. The front panel and block diagram of the implementation program are given in Fig. 7.

The simulations are carried out using MATLAB/SIMULINK software. The main block diagram and the block diagrams of its subsystems used to simulate the control algorithm are given in Fig. 8.

A bidirectional square wave signal with 0.2 m amplitude and 20 s period is used as reference input for the cart position during all test procedure. In the experimental tests, a compensator as given in Eq. (21) is also added to the system to compensate the Coulomb friction of the mechanism.

$$V = V_c + 0.8 \cdot sgn(V_c) \qquad (21)$$

Here the V is the voltage output of the compensator applied to the PWM generator and V_c is the control signal generated from the controller.

Fig. 9 presents the results of simulation and experiment conducted to show the validity of the VMC with the fixed parameters, which lead to the best performance.

TABLE 4. The parameters of the VMC.

Parameter	Value
K_l	0.25
B_l	0.23
K_r	8000
B_r	1150

TABLE 5. The performance specifications of the VMC with fixed parameters.

	Simulated	Experimental
Rise Time	1.1536	1.1636
Settling Time − 5%	1.7283	1.7170
Percentage Overshoot	3.1024%	1.5537%

TABLE 6. The LQR parameters.

Parameter	Value
N	-35
K_x	-35
$K_{\dot{x}}$	-55
K_{θ}	100
$K_{\dot{\theta}}$	19

The fixed parameters of the VMC are determined by trial and error method. The same values given in Table 4 are obtained for the parameters in both the simulation and the experiment.

The performance specifications for controlling the cart position are given in Table 5. The simulated and experimental results are very close to each other. There is no saturation in the DC motor voltage (see Fig. 9-d). The cart reaches the target position in about 1.7 s and there is 1.55% overshoot in the experiment (see Fig.9-a). The θ_r generated by VMC_2, graphs are very smooth in both experiment (see Fig.9-c) and simulation (see Fig.9-b). The proposed VMC with the fixed parameters is able to control the cart while stabilizing the pendulum successfully in both the simulation and the experiment.

The same experiment is conducted again by means of the VMC accompanied with the FPT, which is proposed to improve the performance of VMC in this paper. Additionally an LQR controller is designed for the comparative evaluation. The experiment is also repeated with the LQR controller. Block diagram of the LQR controller is shown in Fig. 10. The best LQR parameters determined by trial and error method are given in Table 6.

Fig. 11 shows comparative results of the experiments conducted by using the VMC with the fixed parameters, the VMC with the FPT, and LQR controller. In addition to the unit step response specifications of the cart position, integral of absolute error (IAE) and integral of time-weighted absolute
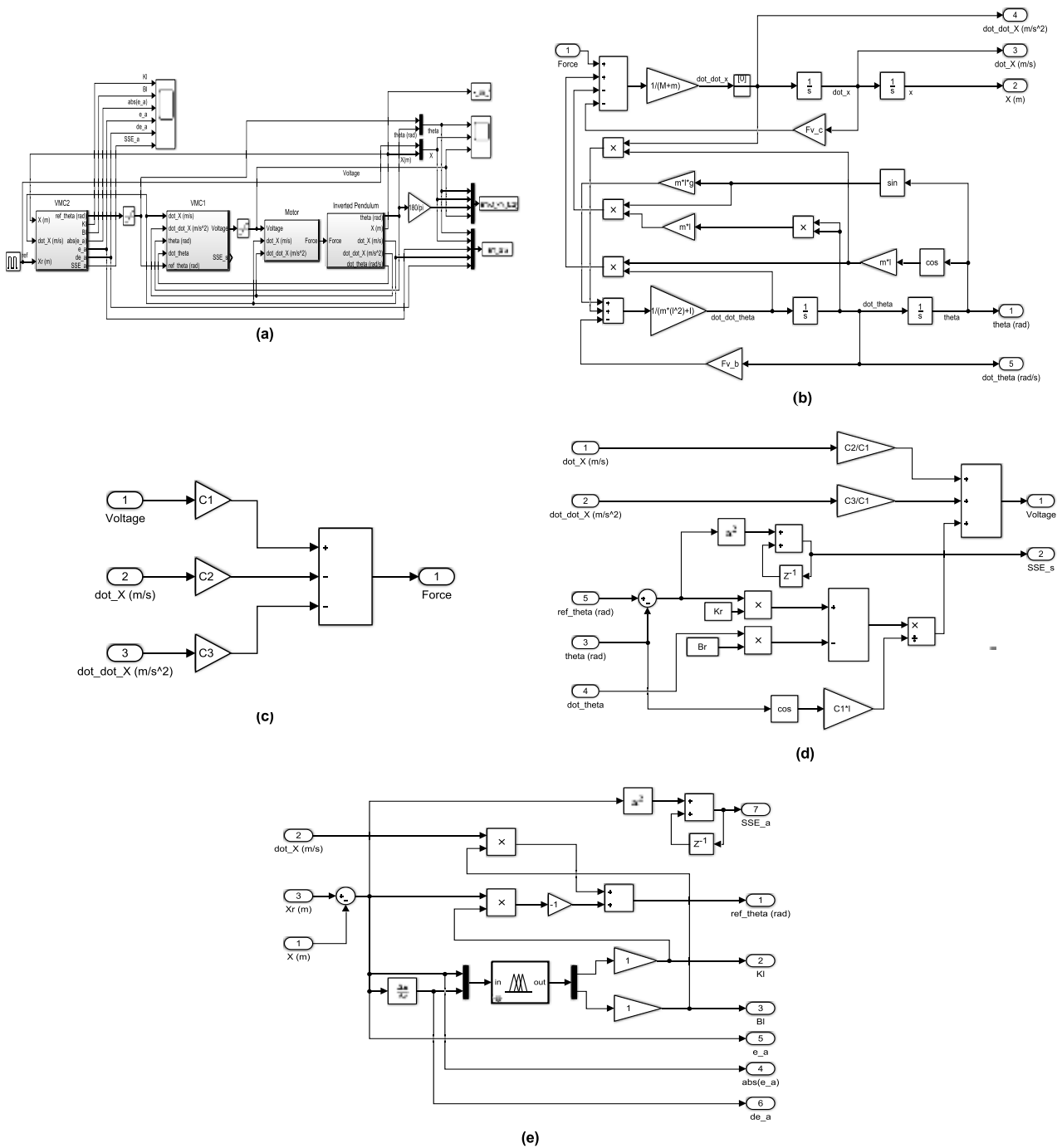
FIGURE 8. The simulation block diagrams of control algorithm. (a) Main block diagram. (b) Block diagram of inverted pendulum subsystem. (c) Block diagram of motor subsystem. (d) Block diagram of VMC1 subsystem. (e) Block diagram of VMC2 subsystem.

error (ITAE), total performance indexes are also calculated for the performance comparison and are given in Table 7.

All the three controllers stabilize the pendulum within ± 1E-3 rad (±0.0573 deg.) (see Fig. 11-b). There is no saturation in the DC motor voltage (see Fig. 11-c). The FPT outputs K_l an B_l are shown in Fig. 11-d. It is clearly seen from the results that the FPT system increased the performance of the VMC significantly. The rise time and

the settling time are decreased from 1.1636 s to 0.6937 s and from 1.7170 s to 1.2899 s, respectively. There is almost no overshoot in experiments with the LQR and the VMC with the FPT. All the performance indexes seen from the Table 7 indicates that the proposed control strategy in this paper controls the cart position better than the LQR controller, which is a widely considered control strategy in the literature.
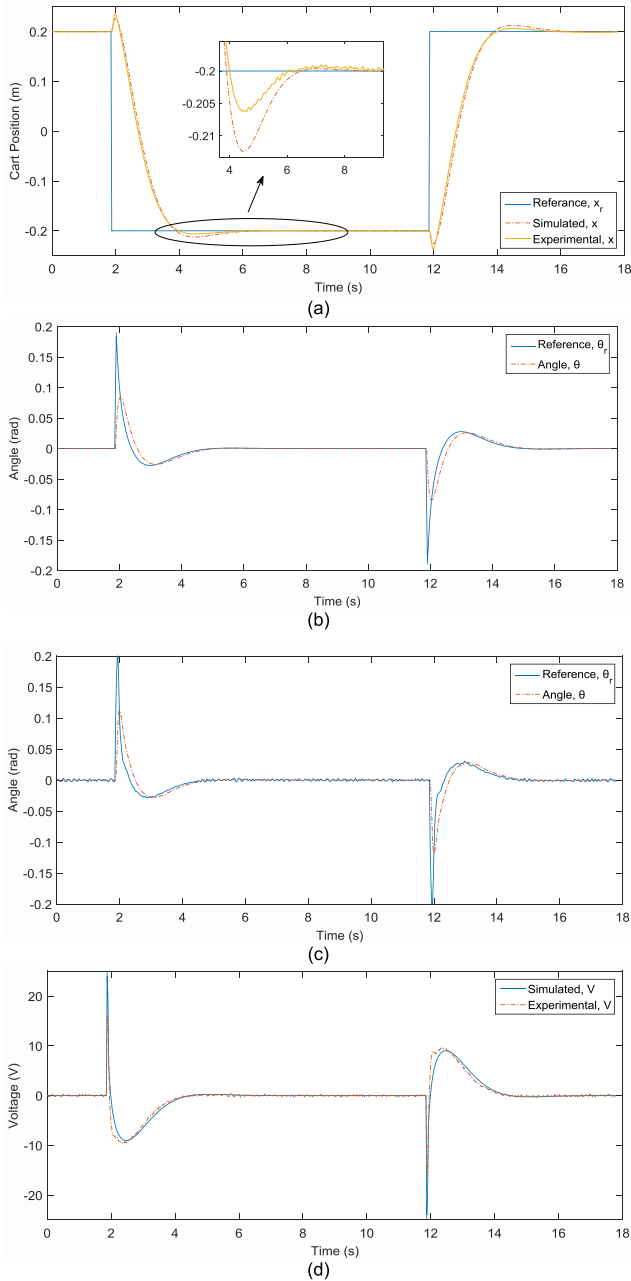
FIGURE 10. Block diagram of the LQR controller.

FIGURE 9. Results of simulation and experiment of VMC with fixed parameters. (a) Time response of the cart (simulated and experimental). (b) Time response of the pendulum angle (simulated). (c) Time response of the pendulum angle (experimental). (d) The voltage applied to the DC motor (simulated and experimental).

FIGURE 11. Comparative results of the experiments using VMC with fixed parameters, VMC with FTP and LQR. (a) Time response of the cart (experimental). (b) Time response of the pendulum angle (experimental). (c) The voltage applied to the DC motor (experimental). (d) Change of virtual element parameters of VMC with FPT (experimental).

Additional experiments are provided to show the external disturbance responses of the proposed control system. The disturbances are applied by human finger from the end of the pendulum while the cart is holden in the centre of the slide. Fig. 12 illustrates the responses of the experiments.

Firstly, small nudge is applied in $+\theta$ direction. Then, the controller makes sudden reaction to damp the disturbance force by moving the cart in the appropriate direction while keeping the pendulum balanced. After that the cart is moved
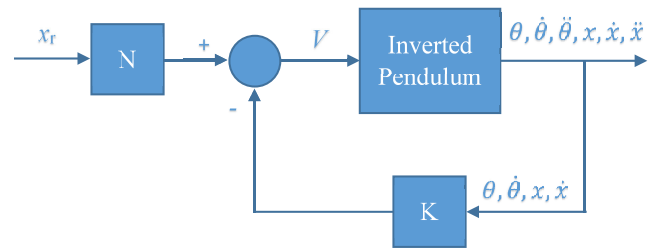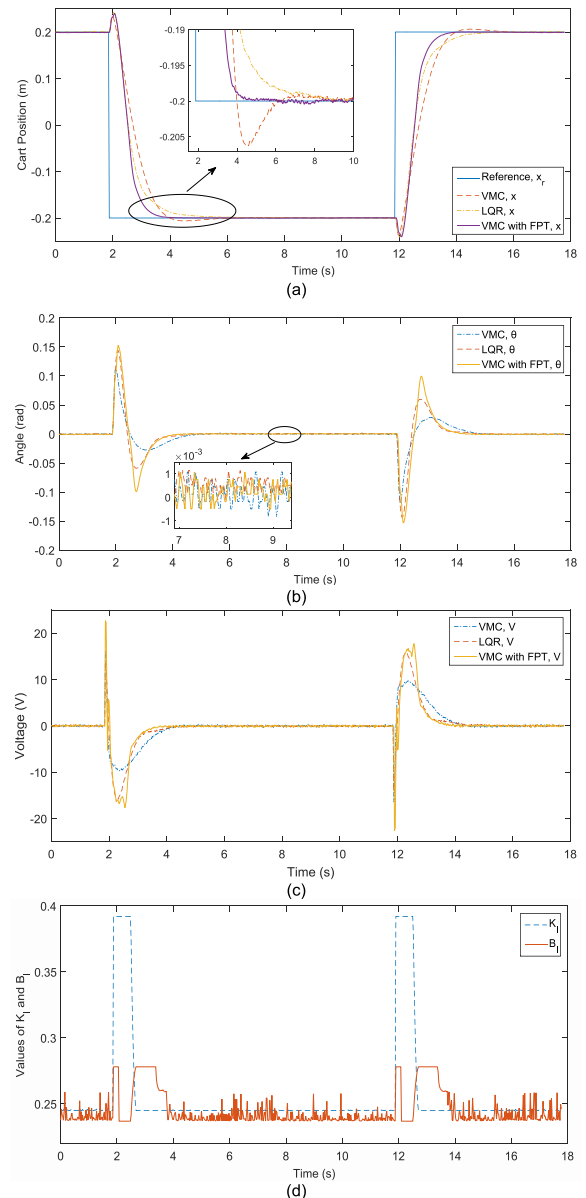
to the centre point and the pendulum is balanced again (see Fig. 12 (a)). Secondly, the pendulum is pushed and pulled for a certain time interval. While the push and pull intervals,

TABLE 7. The performance specifications of the VMC with fixed parameters.

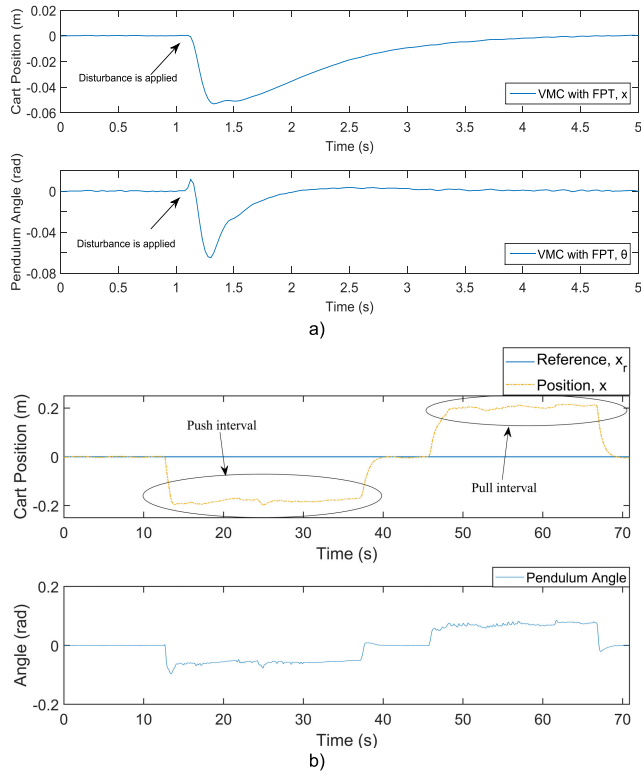|	VMC	LQR	VMC with FPT
Rise Time (s)	1.1636	1.0134	0.6937
Settling Time – 5% (s)	1.7170	1.7964	1.2899
Percentage Overshoot	1.5537%	0.1937%	0.3622%
IAE	0,7591	0,6766	0,6008
ITAE	5,6661	5,0000	4,4261

a)

b)

FIGURE 12. The external disturbance responses of the VMC with FPT. (a) Small nudge is applied to the pendulum. (b) The pendulum is pushed and pulled.
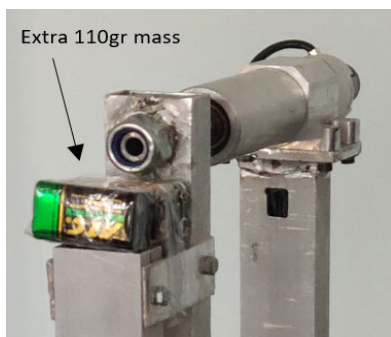

FIGURE 13. A view of the attached extra mass.

the controller balance the applied disturbance forces with the force of gravity by tilting the pendulum in the opposite direction of the disturbance force (see Fig. 12 (b)).

Also, an additional experiment is conducted to show the parameter uncertainties response of the proposed control
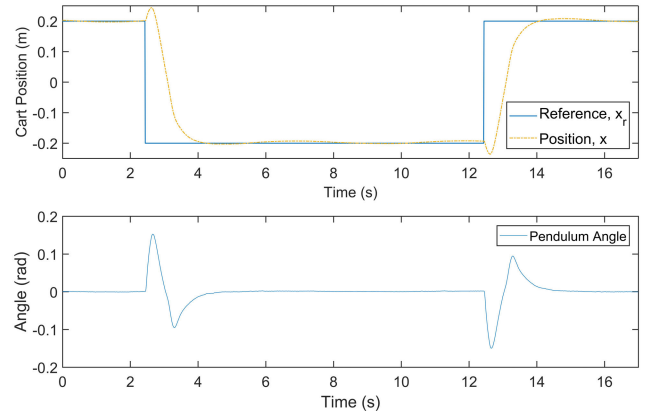

FIGURE 14. The parameter uncertainties responses of the VMC with FPT (an extra 110 gr mass added to the top of the pendulum).
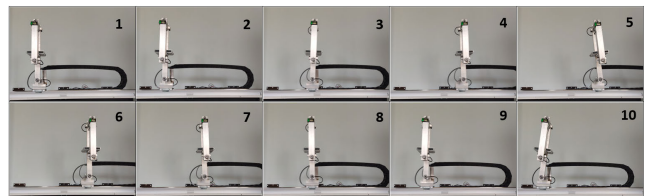

FIGURE 15. Ten sequential images from the uncertainty experiment.
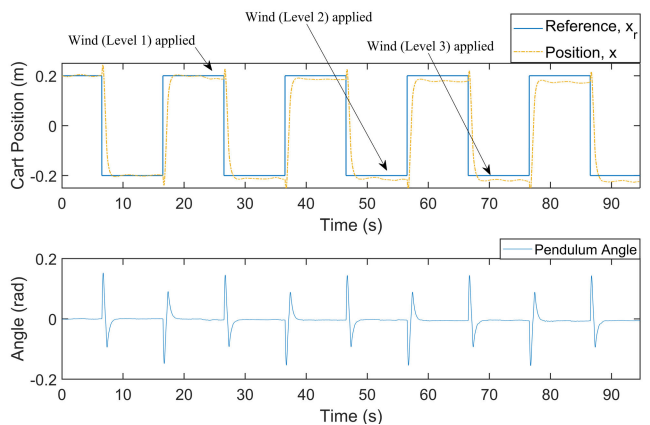

FIGURE 16. The response of the VMC with FPT under strong wind effect.

system by attaching an extra 110 gr mass (5% percent of the pendulum mass) on the top of the pendulum (see Fig. 13).

Fig. 14 illustrates the responses of the experiment. It is clearly seen from Fig. 14 that the proposed controller can achieve the control objective under the presence of parameter uncertainties successfully.

The ten selected sequential images taken from the experiment is shown in Fig. 15.

Another experiment is conducted to show the response of the VMC with FPT controller under strong wind force effect. A three-stage strong wind effect is laterally applied to the inverted pendulum mechanism using a fan with 50W motor operating at three power levels. In order to keep the pendulum in balance, the lateral force exerted by the wind must be

balanced with the force of gravity by tilting the pendulum in the opposite direction of the wind force. Due to the nature of the proposed controller, VMC_2 is the reference generator for VMC_1. It can be clearly seen from Eq. 15 that in order to produce the tilt reference required for the balance, the cart must make a position error in the direction of the wind force. Fig. 16 illustrates the responses of the experiment.

VI. CONCLUSION

Previous works with the virtual model control (VMC) are made on landing gears, legged robots, exoskeletons and especially humanoid robots. Thus, the effects of the parameter changes in the virtual elements are more understandable than those of the classical controllers, optimizing the parameters of the VMC is easy and the design structure of the VMC is intuitive. However, there are no studies on under actuated system control with the VMC. Therefore, a novel implementation of the VMC technique on the under actuated inverted pendulum mechanism is presented. Two cascaded VMCs are designed: one is used to balance the pendulum and the other is used as reference generator for it to control the cart. A Takagi-Sugeno fuzzy parameter tuner is designed to adjust the parameters of the virtual elements. The complete control system is successfully implemented on FPGA based embedded platform, myRIO, in real time. Simulative and experimental results indicated that, the proposed control system is able to keep track of the desired cart position while keeping the pendulum balanced even in the presence of the disturbance. It is shown that the performance of the proposed VMC with the fuzzy parameter tuner is better than that of the LQR controller in terms of lower rise time, settling time, IAE and ITAE. The experimental results show the effectiveness of VMC on under actuated systems. Compared with similar studies [23], [38], [49] in the literature, the proposed control system is tested under more difficult conditions (the position of the cart is tested with a reference position of 0.2 m amplitude). According to the results obtained, maximum overshoot, car position error and pendulum angle error are much less than similar studies. The results give encouragement for the future works on double and triple inverted pendulum control problems. Also the proposed control system can be applied to control problem of tele operating robots [47], [48].

REFERENCES

[1] J.-J. Wang, "Simulation studies of inverted pendulum based on PID controllers," *Simul. Model. Pract. Theory*, vol. 19, pp. 440–449, Jan. 2011.
[2] A. Ghosh, T. R. Krishnan, and B. Subudhi, "Robust proportional-integral-derivative compensation of an inverted cart-pendulum system: An experimental study," *IET Control Theory Appl.*, vol. 6, no. 8, pp. 1145–1152, May 2012.
[3] M. El-Bardini and A. M. El-Nagar, "Interval type-2 fuzzy PID controller for uncertain nonlinear inverted pendulum system," *ISA Trans.*, vol. 53, pp. 732–743, May 2014.
[4] S. Ghoreishi, M. A. Nekoui, and S. O. Basiri, "Optimal design of LQR weighting matrices based on intelligent optimization methods," *Int. J. Intell. Inf. Process.*, vol. 2, no. 1, pp. 57–62, 2011.
[5] L. Wende, H. Ding, and K. Cheng, "An investigation on the design and performance assessment of double-PID and LQR controllers for the inverted pendulum," in *Proc. UKACC Int. Conf. Control*, Cardiff, U.K., Sep. 2012, pp. 190–196.
[6] M. Mahmoodabadi, S. A. Mostaghim, A. Bagheri, and N. Nariman-zadeh, "Pareto optimal design of the decoupled sliding mode controller for an inverted pendulum system and its stability simulation via Java programming," *Math. Comput. Model.*, vol. 57, pp. 1070–1082, Mar. 2013.
[7] J.-J. Wang, "Stabilization and tracking control of X–Z inverted pendulum with sliding-mode control," *ISA Trans.*, vol. 51, pp. 763–770, Nov. 2012.
[8] H. Fukushima, K. Muro, and F. Matsuno, "Sliding-mode control for transformation to an inverted pendulum mode of a mobile robot with wheel-arms," *IEEE Trans. Ind. Electron.*, vol. 62, no. 7, pp. 4257–4266, Jul. 2015.
[9] Z. Zuo, "Non-singular fixed-time terminal sliding mode control of non-linear systems," *IET Control Theory Appl.*, vol. 9, no. 4, pp. 545–552, Feb. 2015.
[10] H. Li and Y. Cai, "On SFTSM control with fixed-time convergence," *IET Control Theory Appl.*, vol. 11, no. 6, pp. 766–773, Apr. 2017.
[11] F. Dai, X. Gao, S. Jing, W. Guo, and Y. Liu, "A two-wheeled inverted pendulum robot with friction compensation," *Mechatronics*, vol. 30, pp. 116–125, Sep. 2015.
[12] A. Rajan, A. A. Kumar, and C. S. Kavitha, "Robust control methods for swing-up and stabilization of a rotary inverted pendulum," in *Proc. Int. Conf. Emerg. Technol. Trends (ICETT)*, Kollam, India, Oct. 2016, pp. 1–6.
[13] M. Muehlebach and R. D'Andrea, "Nonlinear analysis and control of a reaction-wheel-based 3-D inverted pendulum," *IEEE Trans. Control Syst. Technol.*, vol. 25, no. 1, pp. 235–246, Jan. 2017.
[14] S.-J. Huang and C.-L. Huang, "Control of an inverted pendulum using grey prediction model," *IEEE Trans. Ind. Appl.*, vol. 36, no. 2, pp. 452–458, Mar. 2000.
[15] K. Yokoyama and M. Takahashi, "Dynamics-based nonlinear acceleration control with energy shaping for a mobile inverted pendulum with a slider mechanism," *IEEE Trans. Control Syst. Technol.*, vol. 24, no. 1, pp. 40–55, Jan. 2016.
[16] Y.-H. Liu, G.-Z. Cao, S.-X. Tang, X.-S. Cai, and J.-Z. Peng, "Energy-based stabilisation and H∞ robust stabilisation of stochastic non-linear systems," *IET Control Theory Appl.*, vol. 12, no. 2, pp. 318–325, 2018.
[17] S. Kizir, Z. Bingul, and C. Oysu, "Fuzzy control of a real time inverted pendulum system," *J. Intell. Fuzzy Syst.*, vol. 21, nos. 1–2, pp. 121–133, 2008.
[18] J.-X. Xu, Z.-Q. Guo, and T. H. Lee, "Design and implementation of a Takagi–Sugeno-type fuzzy logic controller on a two-wheeled mobile robot," *IEEE Trans. Ind. Electron.*, vol. 60, no. 12, pp. 5717–5728, Dec. 2013.
[19] C.-H. Huang, W.-J. Wang, and C.-H. Chiu, "Design and implementation of fuzzy control on a two-wheel inverted pendulum," *IEEE Trans. Ind. Electron.*, vol. 58, no. 7, pp. 2988–3001, Jul. 2011.
[20] Z. Li, "Adaptive fuzzy output feedback motion/force control for wheeled inverted pendulums," *IET Control Theory Appl.*, vol. 5, no. 10, pp. 1176–1188, 2011.
[21] X. Yang and X. Zheng, "Swing-up and stabilization control design for an underactuated rotary inverted pendulum system: Theory and experiments," *IEEE Trans. Ind. Electron.*, vol. 65, no. 9, pp. 7229–7238, Sep. 2018.
[22] X. Jia, Y. Dai, and Z. A. Memon, "Adaptive neuro-fuzzy inference system design of inverted pendulum system on an inclined rail," in *Proc. 2nd WRI Global Congr. Intell. Syst.*, Dec. 2010, pp. 137–141.
[23] Y. Bibi, O. Bouhali, and T. Bouktir, "Petri type 2 fuzzy neural networks approximator for adaptive control of uncertain non-linear systems," *IET Control Theory Appl.*, vol. 11, no. 17, pp. 3130–3136, 2017.
[24] B. M. Mohan and A. Sinha, "Mathematical models of the simplest fuzzy PI/PD controllers with skewed input and output fuzzy sets," *ISA Trans.*, vol. 47, no. 3, pp. 300–310, 2008.
[25] J. Pratt, A. Torres, P. Dilworth, and G. Pratt, "Virtual actuator control," in *Proc. IEEE/RSJ Int. Conf. Intell. Robots Syst.*, Nov. 1996, pp. 1219–1226.
[26] J. Pratt, C.-M. Chew, A. Torres, P. Dilworth, and G. Pratt, "Virtual model control: An intuitive approach for bipedal locomotion," *Int. J. Robot. Res.*, vol. 20, no. 2, pp. 129–143, 2001.
[27] J. Pratt and G. Pratt, "Intuitive control of a planar bipedal walking robot," in *Proc. Int. Conf. Robot. Automat.*, Leuven, Belgium, May 1998, pp. 2014–2021.
[28] J. Hu, J. Pratt, C.-M. Chew, H. Herr, and G. Pratt, "Adaptive virtual model control of a bipedal walking robot," in *Proc. IEEE Int. Joint Symposia Intell. Syst.*, May 1998, pp. 245–251.
[29] B. J. Stephens and C. G. Atkeson, "Dynamic balance force control for compliant humanoid robots," in *Proc. IEEE/RSJ Int. Conf. Intell. Robots Syst.*, Taipei, Taiwan, Oct. 2010, pp. 1248–1255.

[30] M. Hutter, C. D. Remy, M. A. Hoepflinger, and R. Siegwart, "ScarlETH: Design and control of a planar running robot," in *Proc. IEEE/RSJ Int. Conf. Intell. Robots Syst.*, San Francisco, CA, USA, Sep. 2011, pp. 562–567.

[31] J. Oehlke, M. A. Sharbafi, P. Beckerle, and A. Seyfarth, "Template-based hopping control of a bio-inspired segmented robotic leg," in *Proc. IEEE RAS/EMBS Int. Conf. Biomed. Robot. Biomechatronics (BioRob)*, Singapore, Jun. 2016, pp. 35–40.

[32] M. Ajallooeian, S. Pouya, A. Sproewitz, and A. J. Ijspeert, "Central pattern generators augmented with virtual model control for quadruped rough terrain locomotion," in *Proc. IEEE Int. Conf. Robot. Automat. (ICRA)*, Karlsruhe, Germany, May 2013, pp. 3321–3328.

[33] A. Winkler, I. Havoutis, S. Bazeille, J. Ortiz, M. Focchi, R. Dillmann, D. Caldwell, and C. Semini, "Path planning with force-based foothold adaptation and virtual model control for torque controlled quadruped robots," in *Proc. IEEE Int. Conf. Robot. Automat. (ICRA)*, Hong Kong, May/Jun. 2014, pp. 6476–6482.

[34] G. Zhang, X. Rong, C. Hui, Y. Li, and B. Li, "Torso motion control and toe trajectory generation of a trotting quadruped robot based on virtual model control," *Adv. Robot.*, vol. 30, no. 4, pp. 284–297, 2015.

[35] R. Ekkelenkamp, P. Veltink, S. Stramigioli, and H. van der Kooij, "Evaluation of a virtual model control for the selective support of gait functions using an exoskeleton," in *Proc. IEEE 10th Int. Conf. Rehabil. Robot.*, Noordwijk, The Netherlands, Jun. 2007, pp. 693–699.

[36] H. van der Kooij, B. Koopman, and E. H. van Asseldonk, "Body weight support by virtual model control of an impedance controlled exoskeleton (LOPES) for gait training," in *Proc. 30th Annu. Int. IEEE Conf. (EMBS)*, Vancouver, BC, Canada, Aug. 2008, pp. 1969–1972.

[37] D. Kim and M. Costello, "Virtual model control of rotorcraft with articulated landing gear for shipboard landing," in *Proc. AIAA Guidance, Navigat., Control Conf.*, San Diego, CA, USA, 2016, p. 1863.

[38] A. M. El-Nagar, M. El-Bardini, and N. M. El-Rabaie, "Intelligent control for nonlinear inverted pendulum based on interval type-2 fuzzy PD controller," *Alexandria Eng. J.*, vol. 53, no. 1, pp. 23–32, 2014.

[39] M. I. El-Hawwary, A. L. Elshafei, H. M. Emara, and H. A. A. Fattah, "Adaptive fuzzy control of the inverted pendulum problem," *IEEE Trans. Control Syst. Technol.*, vol. 14, no. 6, pp. 1135–1144, Nov. 2006.

[40] H.-C. Lu, M.-H. Chang, and C.-H. Tsai, "Adaptive self-constructing fuzzy neural network controller for hardware implementation of an inverted pendulum system," *Appl. Soft Comput.*, vol. 11, no. 5, pp. 3962–3975, Jul. 2011.

[41] R. Agrawal and R. Mitra, "Adaptive neuro fuzzy inference structure controller for rotary inverted pendulum," in *Proc. Int. Conf. Adv. Comput.*, 2013, pp. 1163–1170.

[42] Maxon. *RE 50 Ø50 mm, Graphite Brushes, 200 Watt*. Accessed: Sep. 15, 2017. [Online]. Available: https://www.maxonmotor.com/medias/sys_master/root/8825409470494/17-EN-133.pdf

[43] National Instruments. (2017). *myRIO*. [Online]. Available: http://www.ni.com/en-tr/shop/select/myrio-student-embedded-device

[44] C. Iwendi, M. A. Alqarni, J. H. Anajemba, A. S. Alfakeeh, Z. Zhang, and A. K. Bashir, "Robust navigational control of a two-wheeled self-balancing robot in a sensed environment," *IEEE Access*, vol. 7, pp. 82337–82348, 2019.

[45] J. Huang, T. Zhang, Y. Fan, and J.-Q. Sun, "Control of rotary inverted pendulum using model-free backstepping technique," *IEEE Access*, vol. 7, pp. 96965–96973, 2019.

[46] H. O. Erkol, "Optimal PI$^\lambda$D$^\mu$ controller design for two wheeled inverted pendulum," *IEEE Access*, vol. 6, pp. 75709–75717, 2018.

[47] J. Luo, J. Yang, N. Wang, and M. Wang, "Enhanced teleoperation performance using hybrid control and virtual fixture," *Int. J. Syst. Sci.*, vol. 50, no. 3, pp. 451–462, 2019.

[48] C. Yang, J. Luo, Y. Pan, Z. Liu, and C.-Y. Su, "Personalized variable gain control with tremor attenuation for robot teleoperation," *IEEE Trans. Syst., Man, Cybern. A, Syst. Humans*, vol. 48, no. 10, pp. 1759–1770, Oct. 2018.

[49] A. Khan, B. Chatterjee, and C. Dey, "Real time performance evaluation of a self-tuning fuzzy PID controller on an inverted pendulum in crane mode operation," in *Proc. Int. Conf. Intell. Control Power Instrum. (ICICPI)*, Oct. 2016, pp. 22–26.

SABRI BICAKCI (M'14) was born in Balıkesir, Turkey, in 1982. He received the B.S. degree in electronics engineering from Erciyes University, Kayseri, in 2005, and the M.S. degree in electrical and electronics engineering and the Ph.D. degree in mechanical engineering from Balıkesir University, Balıkesir, in 2009 and 2012, respectively. From 2005 to 2015, he was a Research Assistant with the Electrical and Electronics Engineering Department, Balıkesir University, where he has been an Assistant Professor with the Mechatronics Engineering Department, since 2015. His research interests include robotics and control systems.

• • •